Low-temperature magnetic ordering and structural distortions in vanadium sesquioxide V_2O_3

Daniel Grieger and Michele Fabrizio
SISSA, Via Bonomea 265, 34136 Trieste, Italy
(Received 17 February 2015; published 10 August 2015)

Vanadium sesquioxide (V_2O_3) is an antiferromagnetic insulator below $T_N \approx 155$ K. The magnetic order does not consist of only antiferromagnetic nearest-neighbor bonds, possibly excluding the interplane vanadium pairs, as one would infer from the bipartite character of the hexagonal basal plane in the high-temperature corundum structure. In fact, a magnetic structure with one ferromagnetic bond and two antiferromagnetic ones in the honeycomb plane is known experimentally to be realized, accompanied by a monoclinic distortion that makes the ferromagnetic bond inequivalent from the other two. We show here that the magnetic ordering, the accompanying monoclinic structural distortion, the magnetic anisotropy, and also the recently discovered high-pressure nonmagnetic monoclinic phase, can all be accurately described by conventional electronic structure calculations within GGA and GGA+U. Remarkably, our calculations yield that the corundum phase would be unstable to a monoclinic distortion even without magnetic ordering, thus suggesting that magnetism and lattice distortion are independent phenomena, though they reinforce each other. By means of GGA+U, we find a metal-to-insulator transition at a critical U_c. Both metal at $U \leqslant U_c$ and insulator above U_c have the same magnetic order as that actually observed below T_N, but different monoclinic distortions. Reassuringly, the distortion on the insulating side agrees with the experimental one. Our results are in line with DMFT calculations for the paramagnetic phase [A. I. Poteryaev *et al.*, Phys. Rev. B **76**, 085127 (2007)], which predict that the insulating character is driven by a correlation-enhanced crystal-field splitting between e_g^π and a_{1g} orbitals that pushes the latter above the chemical potential. We find that the a_{1g} orbital, although almost empty in the insulating phase, is actually responsible for the unusual magnetic order as it leads to magnetic frustration whose effect is similar to a next-nearest-neighbor exchange in a Heisenberg model on a honeycomb lattice.

DOI: 10.1103/PhysRevB.92.075121 PACS number(s): 71.30.+h, 71.15.Mb, 75.25.−j, 71.27.+a

I. INTRODUCTION

For more than forty years, the phase diagram of chromium/titanium-doped vanadium sesquioxide [1,2] (V_2O_3) has gathered great interest, especially because of its isostructural high-temperature paramagnetic metal to paramagnetic insulator transition, which is by now considered the prototypical realization of a genuine Mott transition, i.e., not corrupted by any symmetry breaking. Relatively less attention has instead been paid on the low-temperature antiferromagnetic phase of V_2O_3. Indeed, within a certain doping/pressure range, vanadium sesquioxide undergoes a magnetic phase transition [3] below a critical Néel temperature T_N [3–5], which is around 155 K for undoped V_2O_3 [6]. Since magnetism in a strongly correlated material is just a side effect of Mott's localization, scientific interest in V_2O_3 has mostly focused so far on the latter phenomenon rather than on the mechanism that produces the experimentally observed magnetic order. Indeed, the magnetic structure in V_2O_3 raises a number of intriguing questions most of which are still awaiting an answer.

In V_2O_3, each vanadium atom has two electrons within the t_{2g} orbitals of the cubic-split d shell, as schematically shown in Fig. 1. In the high-temperature corundum structure, the trigonal field further splits the t_{2g} into a lower e_g^π doublet and a higher a_{1g} singlet. In the extreme Mott localized scenario, the two electrons would occupy the e_g^π orbitals and be coupled into a spin $S = 1$ configuration in accordance with Hund's rules, see Fig. 1. This idealized picture, each e_g^π singly occupied and the a_{1g} empty, is not far from what most recent LDA+DMFT calculations predict [7,8]. If we assume legitimate to discard the a_{1g} contribution to the low-energy processes that control the coupling between the $S = 1$ localized moments, we must conclude that the virtual hopping of e_g^π electrons between nearest-neighbor sites gives rise to a conventional antiferromagnetic superexchange within the honeycomb basal plane, whose bipartite character would then lead to a Néel two-sublattice antiferromagnetism. Moreover, since the e_g^π orbitals are nonbonding along the c axis perpendicular to the hexagonal plane, we would expect an antiferromagnetic order either of the G type (all bonds antiferromagnetic) or the C type (only out-of-plane bonds ferromagnetic), which we shall hereafter denote as "simple" [9] and "layered" antiferromagnetic structures, respectively, see Fig. 2.

In reality, the experimentally observed magnetic structure [5], which we shall refer to as "true" and show in Fig. 2, is completely different. Along the c axis, the two nearest-neighbor vanadium atoms are coupled ferromagnetically, not in disagreement with the above expectation. In contrast, among the three bonds connecting one vanadium atom to its nearest neighbors within the honeycomb basal plane, only two are antiferromagnetic but the remaining one is ferromagnetic. This phase is accompanied by a monoclinic distortion which goes along with the magnetic structure, making one hexagonal bond inequivalent from the other two. However, slightly contradicting results about the exact influence onto the respective bond lengths can be found in literature, from shortening the antiferromagnetic bonds [6,10], as one would reasonably expect, to the opposite [11].

The natural issue that arises is why this complicated "true" magnetic order should be energetically favorable with respect to the "simple" or "layered" structures in view of the additional energy cost of the monoclinic distortion. Up to now, this simple question has still not found a satisfactory answer.

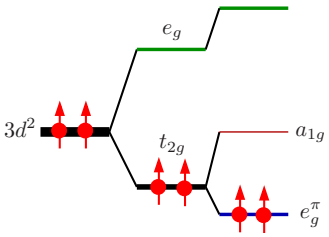

FIG. 1. (Color online) d levels and their occupancy of a hypothetical isolated vanadium atom in the trigonal field of the high-temperature corundum structure.

The first attempt to explain the observed magnetic structure was performed in a series of papers by Castellani, Natoli, and Ranninger (CN&R) [12–14]. Their starting point was not the atomic limit of Fig. 1, but the molecule of two nearest-neighbor vanadium atoms along the c axis, which we shall refer to as a "dimer." The a_{1g} orbitals form a covalent bond along the c axis that falls below the e_g^π levels, see Fig. 3. The lowest electronic configuration consists then of two electrons in a spin-singlet configuration occupying the σ bond, and the remaining two coupled into a spin-triplet configuration within the e_g^π levels. The residual fourfold orbital degeneracy besides the threefold spin degeneracy was exploited to build a spin-orbital Kugel'-Komskii-type [15] of Heisenberg model, whose mean-field solution in a certain parameter range reproduces the observed magnetic structure and simultaneously predicts an orbital ordering. The CN&R's scenario implies that each vanadium has spin $S = 1/2$, while the dimer has $S = 1$. In order to explain the observed magnetic moment larger than one Bohr magneton, CN&R proposed an enhancement mechanism due to the antiparallel polarization of the oxygens as well as an exchange polarization of the a_{1g} electrons [13].

The "dimer" building block was later questioned on the basis of x-ray absorption measurements [16] and of *ab initio* LDA+U calculations [9], both supporting a scenario in which each vanadium is in a spin $S = 1$ configuration rather than spin

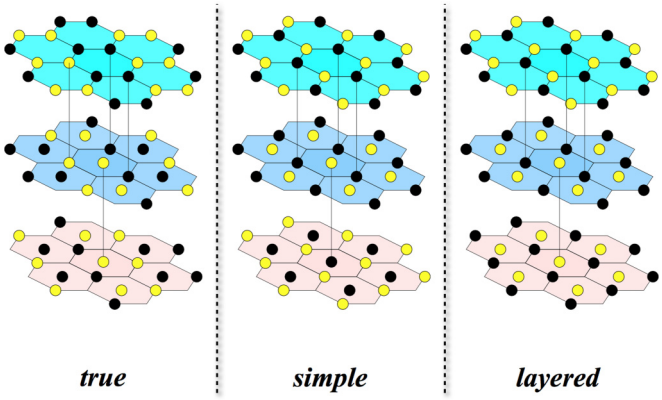

FIG. 2. (Color online) Magnetic structures considered in the calculations, where black and yellow dots correspond to opposite spin vanadiums. The "true" is the one experimentally observed, while "simple" and "layered" represent two-sublattice Neél ordered honeycomb planes coupled antiferromagnetically and ferromagnetically, respectively.

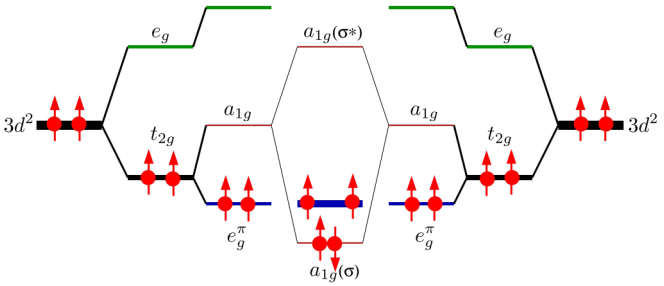

FIG. 3. (Color online) The "dimer" building block of Castellani, Natoli, and Ranninger, with its electronic configuration.

1/2. This conclusion was further reinforced by x-ray scattering measurements showing that the observed moment of 1.2 μ_B has both a spin contribution $2\langle S\rangle \simeq 1.7$ as well as an orbital one $\langle L\rangle \simeq -0.5$ [17]. All these novel results stimulated attempts to reexamine the CN&R model in terms of $S = 2$ dimers (each vanadium in a spin-triplet state) rather than $S = 1$ as in the original formulation, see, e.g., Refs. [18–21], although this list is by no means exhaustive.

At the meantime, the same belief that the V_2 dimer is the relevant building block to explain the magnetic structure started to be questioned [22–24], until most recent LDA+DMFT calculations [7,8] have finally come back to the atomic scenario of Fig. 1 as the most plausible one for the insulating phase of V_2O_3. Nevertheless, important issues remain open, which might escape from very accurate but still approximate techniques like LDA+U or LDA+DMFT [24,25].

An important one is the aforementioned sizable orbital contribution to the magnetic moment [17]. We observe that the t_{2g} orbitals can make available at most an orbital moment $L = 1$. Therefore the observed $|\langle L\rangle| \sim 0.5$ is a substantial part of it, which cannot be justified within the atomic limit of Fig. 1, since the e_g^π alone are not spin-orbit active, but can be explained within the dimer scenario [21,25].

Equally intriguing remains the monoclinic distortion accompanying the magnetic order. As we mentioned, if we assume the atomic limit of Fig. 1 and neglect contributions from a_{1g} orbitals, only "simple" or "layered" magnetic structures can be stabilized. More realistic LDA+U calculations by Ezhov *et al.* [9] show that in the corundum structure the lowest energy magnetic configuration is indeed the "simple" one, lower by 5 K than the "true" structure. Since the monoclinic distortion costs elastic energy, it is not easy to conceive on the basis of these calculations why V_2O_3 would distort to stabilize a phase that in the undistorted crystal is higher in energy. Tight-binding Hartree-Fock calculations by Perkins *et al.* [24] performed with hopping matrix elements of symmetry appropriate to the corundum phase find that the "true" structure can have lower energy than the "simple" one even in the undistorted lattice, though in a quite narrow region of parameter space. Similar conclusions are obtained within the dimer model [18,19].

In summary, in spite of many attempts performed in the last forty years, the real cause of the observed magnetic order and concomitant monoclinic distortion in V_2O_3 is still elusive and we believe it is worth trying to shed further light, which we hope to do in the present study. The approach we shall adopt is

mainly plain density functional theory (DFT) and its DFT+U extension to strong electronic correlations, which is especially suitable for antiferromagnetic insulators. In this sense, this work is partially an extension of the pioneering one by Ezhov *et al.* [9]. Furthermore, model studies are shown to support the findings from these realistic theories.

The paper is organized as follows. Section II summarizes the density functional theory (DFT) picture of V_2O_3 regarding magnetism and structural distortions. Section III enhances this picture by strong electronic correlations as described by DFT+U approaches. Section IV focuses on the orientation of the magnetic moments as described by DFT+U as well as by an analytic picture. Section V finally aims at finding reasons for the type of magnetic ordering realized in V_2O_3 by considering suitable model studies.

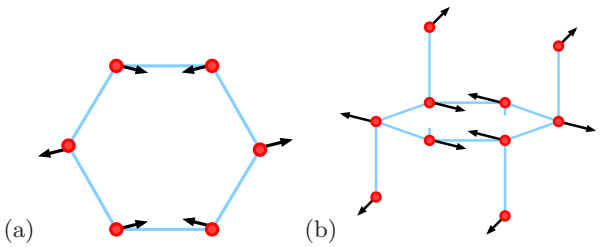

FIG. 4. (Color online) Sketch of the monoclinic distortion occurring in the metallic regime as obtained by GGA (without U): (a) top view onto the honeycomb plane and (b) side view onto the vanadium dimers. Note that the arrows are not perspective but show the movement in the respective view plane.

II. DFT STUDIES

It is obvious that electronic correlations do play a crucial role in the physics of V_2O_3, as demonstrated in detail by several earlier studies [7–9,26], to which the antiferromagnetic ground state makes no exception. However, already density functional theory (DFT) in its generalized-gradient approximation (GGA) to the energy functional (here in its PBE parameterization [27]), in spite of being known to fail for several strongly correlated systems, can give some important insights into this state. It is understood that one cannot expect an accurate description of all the observed properties by plain GGA, but it will be shown to be a useful starting point for all further considerations.

The following DFT calculations have been performed with the QUANTUM ESPRESSO code [28] using ultrasoft pseudopotentials.[1] To account for the monoclinic distortion and magnetic ordering, a supercell containing eight vanadium atoms is used. Its symmetry properties are described by the monoclinic space group $I2/a$ [6,29], whose lattice vectors $(\mathbf{a}_m,\mathbf{b}_m,\mathbf{c}_m)$ can be built from the original high-temperature corundum structure lattice vectors $(\mathbf{a}_\mathrm{H},\mathbf{b}_\mathrm{H},\mathbf{c}_\mathrm{H})$ in hexagonal notation as follows:

$$\begin{pmatrix}\mathbf{a}_m\\ \mathbf{b}_m\\ \mathbf{c}_m\end{pmatrix} = \begin{pmatrix}\frac{2}{3} & \frac{4}{3} & \frac{1}{3}\\ 1 & 0 & 0\\ \frac{1}{3} & \frac{2}{3} & -\frac{1}{3}\end{pmatrix}\begin{pmatrix}\mathbf{a}_\mathrm{H}\\ \mathbf{b}_\mathrm{H}\\ \mathbf{c}_\mathrm{H}\end{pmatrix}. \quad (1)$$

If not stated otherwise, the length of the unit vectors will not be altered throughout the following calculations, but retained at its experimentally reported value at ambient conditions [29].

A. The nonmagnetic solution

The most basic GGA setup that can be built for V_2O_3 is a calculation which is constrained to give a nonmagnetic result. If done in the enlarged eight-site unit cell and allowing for relaxation of the atomic positions, its solution has the noteworthy peculiarity that it incorporates a monoclinic distortion. In spite of the elastic energy cost that is associated to any kind of lattice distortion, the energy gain compared to the relaxed nonmagnetic corundum structure is as large as 25 meV per vanadium atom.

The effects of this distortion are sketched in Fig. 4, which compares the monoclinic distorted structure with the relaxed corundum structure. The distortion is characterized by a shortening of one set of nearest-neighbor bonds in the hexagonal a_H-b_H plane (the bonds drawn horizontally in Fig. 4), therewith enlarging the other two. This movement also leads to a tilting of the vanadium dimers, which, together with a small out-of-plane movement, enlarges them slightly. The above-mentioned large energy gain corresponds to a substantial lattice distortion, with the length of the shortened bond in the a_H-b_H plane of 2.56 and thus even slightly smaller than that of the vanadium dimer along the c_H direction of 2.63 Å. Comparing with the length of the enlarged bonds in the a_H-b_H plane of about 3.0 Å, one notices that the structure becomes similar to an array of 1D chains, each of them running along the dimer and the short bond in the hexagonal plane.

Anticipating results of the next section, we mention that the same kind of distortion occurs in the antiferromagnetic metal phase. However, if GGA is supplemented by a Hubbard U, above a threshold value, an antiferromagnetic insulating phase is established, which still has a monoclinic distortion but with two bonds shortened and one lengthened, hence opposite to that in the metal phases, either nonmagnetic or antiferromagnetic. We remark that the occurrence of a monoclinic structural change in the nonmagnetic solution implies that magnetism and monoclinic distortion are rather unrelated phenomena.

Although such a monoclinic nonmagnetic metal phase is unstable against magnetism, as we shall show in the next section, it is nevertheless of interest in view of the recent discovery of a high-pressure monoclinic metal phase [30] that is actually not dissimilar to what we just found. It is therefore worth investigating the mechanisms that may drive such a distortion.

We believe that the monoclinic distortion is actually driven by a Fermi surface nesting of the corundum band structure. Indeed, the central sheet of the whole Fermi surface, shown in Fig. 5(a) and calculated with the structural data of Ref. [29] corresponding to the high-temperature paramagnetic metal, has nesting properties compatible with an instability towards a monoclinic distortion with a unit cell doubling. This is quite evident by looking at cut planes as shown in Fig. 5(b).

[1] V.pbe-n-van.UPF and O.pbe-van_ak.UPF from http://www.quantum-espresso.org.

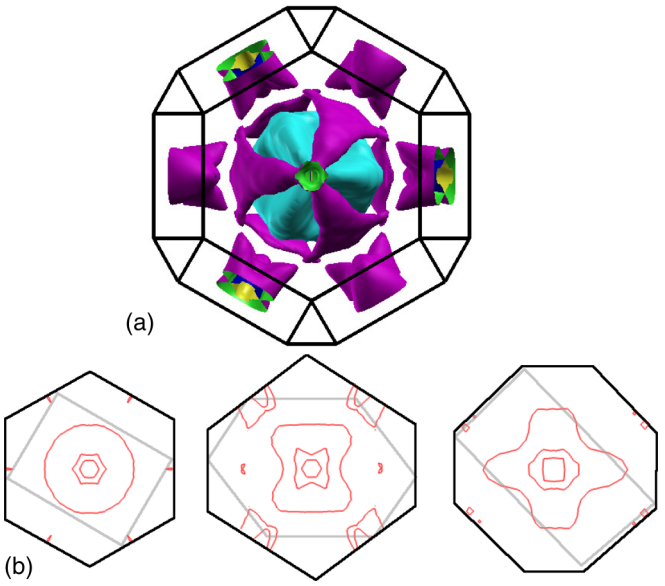

FIG. 5. (Color online) (a) Fermi surface of nonmagnetic metallic corundum structure V_2O_3 with relaxed atomic positions, seen along the crystallographic c_H direction, equivalently the Cartesian z axis. (b) Projections of the Fermi surface onto planes that are obtained by rotating around the Cartesian y axis of (a). While the vertical axis corresponds to the Cartesian y direction, the horizontal axis is the Cartesian x direction (left); rotated about 40° with respect to the former, so that it represents the direction towards a next-nearest-neighbor atom in the adjacent hexagonal plane (middle); perpendicular to the latter (right). The black lines indicate the Brillouin zone boundary of the corundum structure, the grey lines its shape for the doubled monoclinic cell.

While the aforementioned sheet looks almost circular in the honeycomb plane of vanadium atoms, relatively large regions of parallel surfaces can be identified by slightly tilting the cut plane.

An interesting question is whether this nesting is stable against doping. The classical phase diagram [1,2] of V_2O_3 suggests that the monoclinic distortion (as accompanied by the magnetic ordering) is suppressed by large titanium doping, while being almost unaffected by chromium doping. We can estimate the effects of doping by means of energy isosurfaces similar to the Fermi surface of stochiometric V_2O_3, but describing a slightly enlarged (chromium doping) or reduced (titanium doping) total number of electrons. This is done in Fig. 6, which shows that titanium doping tends to shrink the Fermi surface driving the system away from the nesting condition, unlike what happens with chromium doping. In spite of the simplicity of this approach, which lacks subtle correlation effects, it is remarkable that the observed trend is compatible with experiments.

In order to better uncover the driving physical mechanism, the band structures in the enlarged eight-atom unit cell shown in Fig. 7 are particularly enlightening. The chosen path through the Brillouin zone pertaining to the enlarged eight-atom monoclinic cell starts from the point $V = (0, \frac{1}{4}, -\frac{1}{4})$ in relative reciprocal coordinates (compatible with the magnetic order), moves further to Γ and along the vanadium dimer ($\Gamma - A$ direction), further goes in the plane perpendicular thereto at

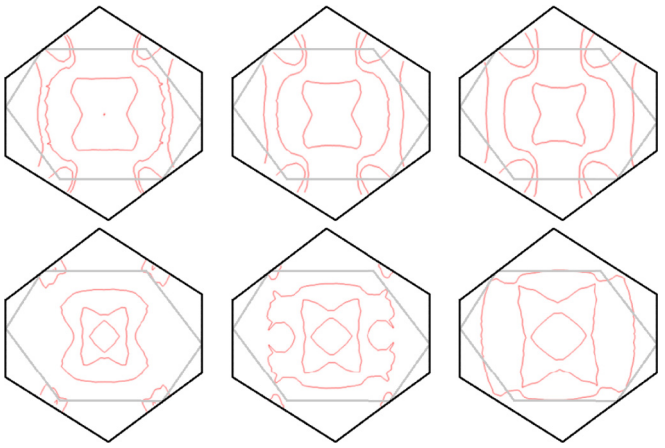

FIG. 6. (Color online) Projections of Kohn-Sham energy isosurfaces of nonmagnetic metallic corundum structure V_2O_3 with relaxed atomic positions onto a plane as in the middle column of Fig. 5(b). The isovalues are chosen to represent roughly values of 5%, 10%, and 15% (from left to right) titanium doping (top row) and chromium doping (bottom row). The black lines indicate the Brillouin zone boundary of the corundum structure, the grey lines its shape for the doubled monoclinic cell.

the "upper" ($k_z = \frac{1}{2}$) edge of the Brillouin zone (A-M), back to the original hexagonal $a_H b_H$ plane at $k_z = 0$ (M-Y) and continues in this plane (Y-Γ-L).

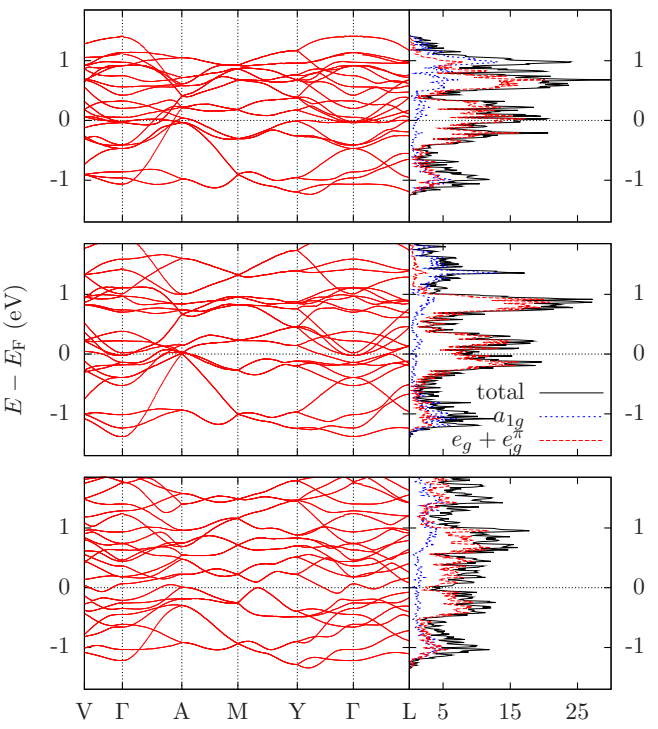

FIG. 7. (Color online) Band structure (left) and projected density of states (right) from GGA of nonmagnetic corundum structure V_2O_3 with atomic positions determined experimentally for the paramagnetic metallic phase [29] (top), GGA-relaxed atomic positions in the corundum structure (middle) and GGA-relaxed atomic positions allowing for a monoclinic distortion (bottom).

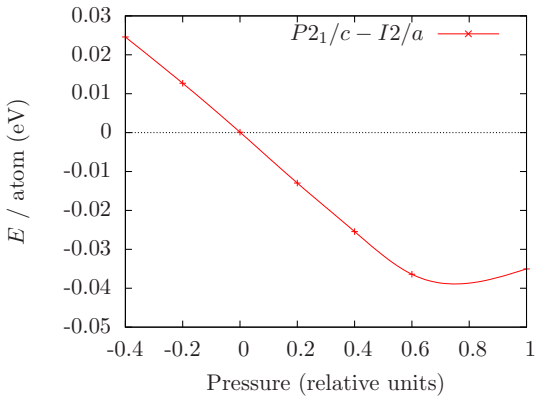

FIG. 8. (Color online) Total energy difference of the $P2_1/c$ and $I2/a$ phases of monoclinic V_2O_3, as a function of the applied pressure. The relative units of the pressure axis correspond to the reported values in the corundum structure at ambient conditions [29] (0.0) and the experimentally reported values of the high-pressure phase transition from $I2/a$ to $P2_1/c$ [30] (1.0).

Starting from the well-known [31,32] GGA low-energy density of states and band structure of the corundum nonmagnetic metal, as displayed in the top row of Fig. 7, one immediately notices a large density of states directly at the Fermi energy, due to almost flat bands near Γ. As expected, relaxation of the atomic positions within the corundum structure (middle row of Fig. 7) partially reduces this instability, and furthermore leads to a reduction of the splitting between e_g^π and high-energy e_g [33]. However, allowing for a monoclinic distortion (bottom row of Fig. 7) further stabilizes the system by splitting the flat bands around Γ and opening a pseudogap at the Fermi energy. We mention that the undistorted structure is not even metastable, but corresponds to a saddle point in the total energy.

We finally mention that the above monoclinic nonmagnetic metal phase is not exactly equivalent to that observed at high pressure in Ref. [30], which is characterized by a further symmetry lowering from $I2/a$ to $P2_1/c$. Figure 8 shows that this symmetry reduction can also be seen in GGA upon simulating pressure by a decrease of the unit cell volume. Both phases $I2/a$ and $P2_1/c$ are minima of the total energy. At ambient pressure, $I2/a$ has a slightly lower energy than $P2_1/c$, but the situation is reverted already applying small pressure. Therefore the transition from $I2/a$ to $P2_1/c$ would occur according to GGA at significantly lower pressures than reported experimentally [30]. We believe that this is an artifact due to GGA underestimation of electronic correlations. Indeed, the $P2_1/c$ structure in GGA is characterized by a charge disproportionation between inequivalent vanadium atoms, which is hindered by electronic correlations.

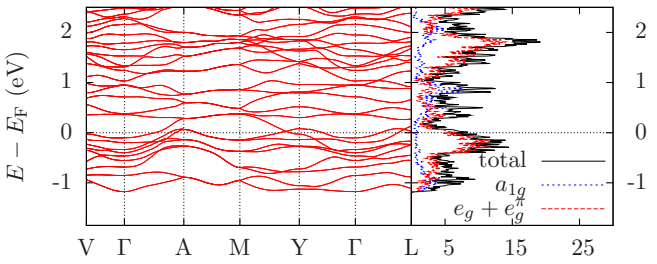

FIG. 9. (Color online) Band structure (left) and projected density of states (right) of true antiferromagnetic V_2O_3 from GGA.

B. Magnetic solutions

Allowing for magnetism in the framework of spin-polarized GGA, Table I shows that the nonmagnetic GGA solution described in the previous subsection is unstable compared to all of the magnetic solutions. Likewise, the energy gain due to its monoclinic distortion is significantly smaller than the energy gain due to magnetic exchange.

Comparing the different possible magnetic orderings, an important result that we find is the stability of the "true" antiferromagnetic ordering already in GGA. Note that this requires relaxation of the atomic positions within the crystal cell. Also this relaxation of the "true" antiferromagnetic structure reveals a monoclinic distortion similar to the experimentally observed one and similar (but smaller) to the one described above for the nonmagnetic solution. Note that both the other two investigated antiferromagnetic configurations ("layered" and "simple") remain in an undistorted corundum structure even allowing for structural relaxation. This can also be expected by symmetry considerations of the magnetic structure, recalling that the magnetic exchange energy gain is significantly larger than an energy gain of the structural distortion. This underlines the fact that the monoclinic instability, which we showed occurs even in the nonmagnetic solution, is strengthened by the "true" antiferromagnetic exchange at least in the metallic regime, while changing sign at the transition to the antiferromagnetic insulating state as will be shown later.

As can be seen from the low-energy density of states and band structure shown in Fig. 9, the main drawback is that pure GGA cannot describe the insulating behavior of the magnetic

TABLE I. Comparison of some basic quantities, calculated for the different antiferromagnetic configurations of V_2O_3 within plain GGA. Energies are given relative to the respective "simple" phase.

	"simple"	"true"	"layered"	nonmagnetic
Experimental corundum structure				
Total GGA energy (meV/V atom)	0	− 4.1	− 5.2	179.6
Absolute magnetization (μ_B/V atom)	1.53	1.57	1.54	0
Relaxed structures				
Total GGA energy (meV/V atom)	0	− 12.2	− 7.9	112.1
Absolute magnetization (μ_B/V atom)	1.47	1.55	1.49	0

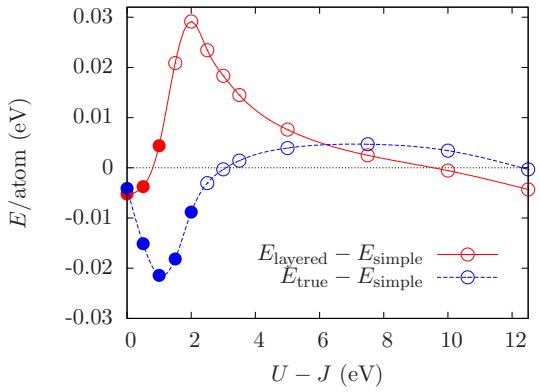

FIG. 10. (Color online) Phase stability comparison in the experimentally determined corundum structure of V_2O_3 within GGA+U. Closed circles indicate metallic, open circles indicate insulating solutions.

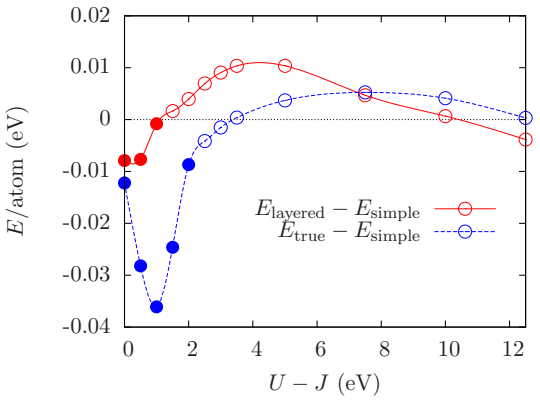

FIG. 11. (Color online) Phase stability comparison in the relaxed structure of V_2O_3 within GGA+U. Closed circles indicate metallic solutions of the layered/true phase, open circles indicate insulating solutions thereof.

structure. This is the expected result in view of the importance of strong electronic correlations in V_2O_3. Furthermore, one notices that the splitting between a_{1g} and e_g^π turns out to be small enough that all orbitals from the t_{2g} block have a similar filling (with the a_{1g} occupation slightly smaller than each e_g^π). This gives rise to a spin magnetic moment of $\sim 1.5\mu_B$ (see Table I), thus slightly smaller than the observed experimental value, which we recall is $\sim 1.7\mu_B$ once corrected by the orbital contribution.

III. DFT+U STUDIES

Since the antiferromagnetic insulating state is the ground state of V_2O_3, one can expect to gain insight into the effects of strong electronic correlations already from a simple method like GGA+U. Here, the simplified version of Cococcioni and de Gironcoli [34] in the QUANTUM ESPRESSO package is put into practice, which implies the use of only one effective parameter $U - J$ and a fully localized limit (FLL) double-counting correction.

Since the actual value of the parameter $U - J$ is *a priori* unknown, Fig. 10 compares the stability of each of the possible magnetic structures in terms of their total energy for a wide parameter range. This calculation is performed in the experimental atomic positions in the unrelaxed corundum structure [29], nevertheless already shows that a small $U - J$ is able to stabilize the "true" antiferromagnetic phase, whereas for large interactions the "simple" and "layered" structures become more stable.

The relaxation of the structural parameters within GGA+U further stabilizes the "true" antiferromagnetically ordered phase and extends its stability region, as shown in Fig. 11. We observe that the energy gain of the "true" magnetic order with respect to the next lying one in the unrelaxed structure is comparable to the 25 meV gain of the nonmagnetic solution upon allowing for a monoclinic distortion, see Figs. 10 and 11. Therefore the "true" magnetic order and the monoclinic distortion, even though independent phenomena, nevertheless reinforce each other. It is thus not surprising that the onset of magnetism and the monoclinic distortion occur roughly at the same temperature T_N, with the latter slightly preceding the former [35,36].

As anticipated, above $U - J \simeq 2.0$ eV, the "true" antiferromagnetic state turns from metallic into insulating, which sets between 2.0 and 4.0 eV the range of $U - J$ values that reproduce within GGA+U the magnetic and conducting properties of the actual material. Figure 12 shows the GGA+U Kohn-Sham band structure and density of states projected onto vanadium d-orbitals for $U - J = 3.0$ eV, which we assume to be a realistic estimate.

It turns out that the GGA+U realization of the insulating phase corresponds to the straightforward solution of occupied e_g^π orbitals and almost empty a_{1g} one, thus implying an $S = 1$ spin configuration. As mentioned, this is in line with, e.g., the U-induced paramagnetic Mott metal-insulator transition in DMFT [7], though still a matter of debate, for instance, because neither GGA+U nor single-site DMFT explicitly includes intersite interactions, which would typically stabilize the atomic dimer [24,25].

This scenario is further confirmed in Fig. 13, where we plot the occupation numbers in the crystal field basis that diagonalizes the GGA+U occupation matrix. We mention that, since these orbitals are not strongly localized on a single vanadium atom, the total occupation is not precisely 2. The depletion of the a_{1g}-like crystal-field basis orbital with increasing values of $U - J$ in favor of e_g^π-like orbitals is evident. A noteworthy jump occurs at the metal-insulator

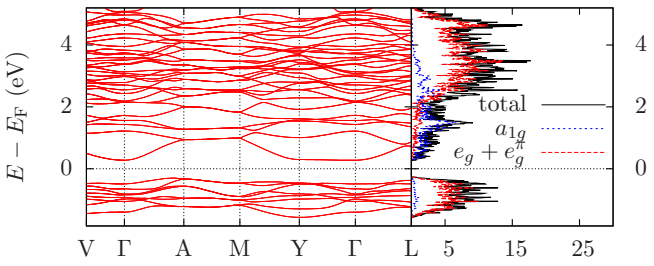

FIG. 12. (Color online) Band structure (left) and projected density of states (right) of true antiferromagnetic V_2O_3 from GGA+U at $U - J = 3.0$ eV.

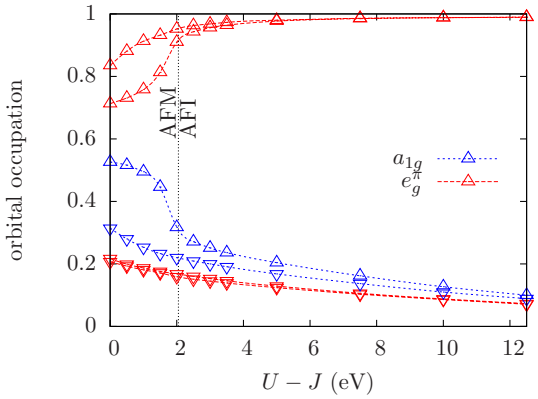

FIG. 13. (Color online) Crystal field basis occupation numbers (eigenvalues of the GGA+U local density matrix) per vanadium d orbital as a function of $U - J$ in the relaxed true antiferromagnetic phase of V_2O_3. Triangles pointing up indicate the majority spin channel, triangles pointing down the minority spin channel. As before, AFM and AFI stand for antiferromagnetic metal and insulator, respectively.

transition, with the above-mentioned scenario of a majority-spin a_{1g} orbital that is almost half-filled below and almost empty above.

One remarkable effect of the monoclinic distortion and the magnetic ordering is the lifting of the degeneracy between the two e_g^π orbitals, which is particularly strong in the (unphysical) magnetic metallic regime, but still present in the magnetic insulating one. It is a direct consequence of the breaking of the threefold rotational symmetry of the vanadium planes with magnetic order or structural distortion, and therefore does not occur for the other investigated magnetic structures that do not break such symmetry.

The inequality between the two e_g^π orbitals, more accentuated the smaller $U - J$, also shows up into different lengths of the two antiferromagnetic in-plane nearest-neighbor bonds, as shown in Fig. 14, to such an extent that, in the metal phase $U - J < 2$ eV, one of the antiferromagnetic bonds is the longest. This is qualitatively the same effect as

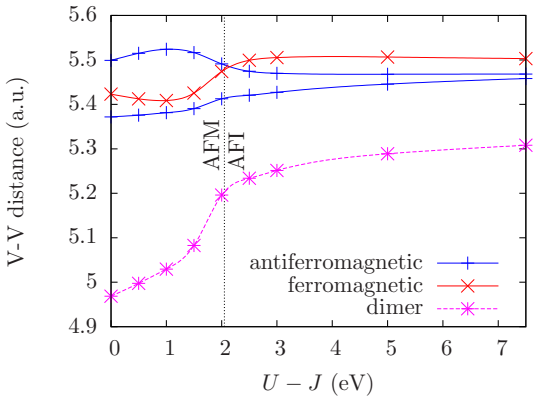

FIG. 14. (Color online) Nearest-neighbor vanadium distances from relaxation in the "true" antiferromagnetic structure, indicating the monoclinic distortion. AFM and AFI stand for antiferromagnetic metal and insulator, respectively.

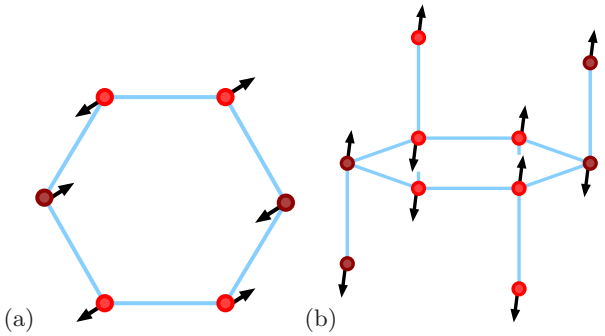

FIG. 15. (Color online) Sketch of the effects of the monoclinic distortion occurring in the antiferromagnetic insulating regime as provided by GGA+U: (a) top view onto a honeycomb plane and (b) side view onto the vanadium dimers. The different colors used for the vanadium atom positions correspond to the different spin orientations (up/down). Note that the arrows are not perspective, but show the movement in the respective view plane.

in the nonmagnetic metallic regime described in Sec. II A. Consequently, for $U - J < 2$ eV, the monoclinic distorted structure corresponds to the one shown in Fig. 4. On the contrary, above $U - J = 2$ eV, i.e., in the realistic insulating phase, all nearest-neighbor vanadium distances shown in the same Fig. 14 are compatible with the observed monoclinic distortion and with the intuitive expectation of elongated ferromagnetic bonds and shortened antiferromagnetic ones. This behavior is illustrated in Fig. 15, which again compares the obtained monoclinic distorted structure (here at $U = 3$ eV) with the relaxed corundum structure. In the figure, horizontal and vertical bonds are ferromagnetic. We note that the in-plane movement is not parallel to any of the bonds, so that a small difference between the lengths of the two in-plane antiferromagnetic bonds persists also in the insulating side. This difference tends to become smaller with increasing U. In the out-of-plane direction, in addition to the rotation of the vanadium dimers caused by the in-plane movement, one can observe a further increase of the vanadium dimer length by an out-of-plane movement. This is not exclusively a feature of the monoclinic distortion, but also of the increased value of U. Indeed, the dimer stretching grows inversely proportional to the a_{1g} occupancy if less than $1/2$. The reason is that, when the a_{1g} occupation drops below $1/2$, the bonding orbital within each dimer, see Fig. 3, loses electrons so that the strength of the bond diminishes hence its length increases. Therefore we expect that the dimer stretching should be barely visible when the monoclinic distortion first appears, since it is only quadratic in the small tilting angle of the dimers that characterizes that distortion [6], but should become more pronounced as the a_{1g} occupancy drops down at the metal-insulator transition. This is in fact in accordance with the experimental data of Ref. [35].

IV. MAGNETIC ANISOTROPY

Already the original 1970's work by Moon [5] pointed out that the magnetic moments are oriented with a certain angle towards the crystallographic c direction. Such a magnetic anisotropy is, at first glance, not expected for a light element like vanadium. However, for similar compounds like

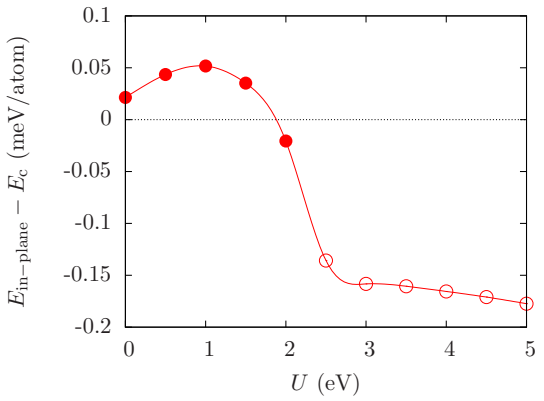

FIG. 16. (Color online) GGA+U energy difference of "true" antiferromagnetic solutions with a spin orientation in the honeycomb plane and in the c direction (perpendicular thereto) as a function of the Hubbard parameter U. Closed circles indicate metallic solutions, while open circles indicate insulating solutions.

vanadium spinels, values of spin-orbit coupling in the range of 13–20 meV have been reported [37–40], which makes a DFT calculation including relativistic effects (spin-orbit coupling) and noncollinear magnetism worth trying. To this end, the implementation thereof [41] in QUANTUM ESPRESSO has been used with a fully relativistic pseudopotential[2] and the rotationally invariant GGA+U formulation of Liechtenstein *et al.* [42]. Due to the high computational demands of such a calculation, no further relaxation of the structural parameters has been done, but values of the monoclinically distorted collinear-antiferromagnetic structure relaxed without U have been used.

Figure 16 shows the energy difference between GGA+U solutions with magnetic moments oriented in the honeycomb plane ($E_{\rm in-plane}$) and oriented perpendicular thereto (E_c), i.e., in the crystallographic c direction. A first result is that, without electronic correlations, i.e., at the GGA level, the c-axis alignment is favored, although with a tiny energy difference. However, upon increasing U, and specifically above the metal-insulator transition, the in-plane orientation becomes more stable. Indeed, there is a close connection between the change from easy axis to easy plane and the a_{1g} depletion that occurs at the metal-insulator transition, which can be illustrated by a simple model calculation.

Let us assume an isolated vanadium in the trigonal crystal field. A suitable basis set for the t_{2g} manifold (with corundum symmetry) can be written (the sign is related to the multiple vanadium atoms per unit cell):

$$\begin{aligned} |a_{1g}\rangle &= |d_{3z^2-r^2}\rangle, \\ |e_{g1}\rangle &= \pm\sqrt{\frac{2}{3}}\,|d_{xy}\rangle + \sqrt{\frac{1}{3}}\,|d_{xz}\rangle, \\ |e_{g2}\rangle &= -\sqrt{\frac{2}{3}}\,|d_{x^2-y^2}\rangle \mp \sqrt{\frac{1}{3}}\,|d_{yz}\rangle. \end{aligned} \tag{2}$$

[2]V.rel-pbe-spnl-rrkjus_psl.1.0.0.UPF from the PSLibrary of http://www.quantum-espresso.org.

We have used a slightly different convention from CN&R [12,13]. Specifically, we have assumed that the wave functions of the two vanadium atoms, which are related by the transformation $C_2(x,y,z) \to (-x,y,-z)$, transform into each other. In addition, the y axis is assumed to correspond to the monoclinic b axis, so that the x-z plane is also the monoclinic a-c one. We observe that the angular momentum operators on the basis of Eq. (3) read

$$\begin{aligned} \hat{L}_x &= \pm i\,|e_{g2}\rangle\langle a_{1g}| \mp i\,|a_{1g}\rangle\langle e_{g2}|, \\ \hat{L}_y &= i\,|e_{g1}\rangle\langle a_{1g}| - i\,|a_{1g}\rangle\langle e_{g1}|, \\ \hat{L}_z &= \pm i\,|e_{g2}\rangle\langle e_{g1}| \mp i\,|e_{g1}\rangle\langle e_{g2}|. \end{aligned}$$

Using the representation $|n_{a_{1g}},n_{e_{g1}},n_{e_{g2}};S_z\rangle$ to denote two electrons coupled into a spin triplet with z component $S^z = -1,0,1$ and occupying the single-particle states (3) with occupation $n_i = 0,1$ such that $\sum n_i = 2$, we define the new states

$$\begin{aligned} |1,S_z\rangle &= -\sqrt{\frac{1}{2}}\,(|1,0,1;S_z\rangle \mp i|1,1,0;S_z\rangle), \\ |0,S_z\rangle &= |0,1,1;S_z\rangle, \\ |-1,S_z\rangle &= \sqrt{\frac{1}{2}}\,(|1,0,1;S_z\rangle \pm i|1,1,0;S_z\rangle), \end{aligned} \tag{3}$$

which are actually eigenstates of the z component of the angular momentum operator L_z projected onto the t_{2g} manifold that effectively realizes an $l = 1$ representation, i.e., $L_z\,|M,S_z\rangle = M\,|M,S_z\rangle$, with $M = -1,0,1$. The spin-orbit coupling projected onto the basis (3) reads

$$H_{\rm SOC} = \frac{\lambda_{\rm SOC}}{2}\,(2\,S_z\,L_z + S^+\,L^+ + S^-\,L^-), \tag{4}$$

where $L^\pm$ in the basis (3) has the same expressions as for $l = 1$ angular momentum operators, while the trigonal crystal field can be written as

$$H_{\rm tr} = 3V_{\rm tr}\left(L_z^2 - \tfrac{2}{3}\right). \tag{5}$$

One can easily realize that, for $V_{\rm tr} = 0$, the lowest energy state at $\lambda_{\rm SOC} \neq 0$ is fivefold degenerate, corresponding to two d electrons coupled according to the Hund's rules to $S = 1$, $L = 3$, and $J = 2$. Conversely, for $\lambda_{\rm SOC} = 0$ but $V_{\rm tr} \neq 0$, the lowest energy state $|0,S_z\rangle$ is an orbitally nondegenerate spin triplet.

However, when both parameters are finite with $\lambda_{\rm SOC} \ll V_{\rm tr}$, the lowest energy state is

$$|0\rangle \equiv \cos\theta\,|0,0\rangle - \frac{\sin\theta}{\sqrt{2}}\,(|1,1\rangle + |-1,-1\rangle), \tag{6}$$

with

$$\tan 2\theta = \frac{2\sqrt{2}\,\lambda_{\rm SOC}}{3V_{\rm tr} + \lambda_{\rm SOC}},$$

followed by the doublet

$$|\pm 1\rangle \equiv \cos\phi\,|0,\pm 1\rangle - \sin\phi\,|\mp 1,0\rangle, \tag{7}$$

with $\tan 2\phi = 2\lambda_{\rm SOC}/3V_{\rm tr}$.

If we regard the three states $|0\rangle$ and $|\pm 1\rangle$ as the effective $S = 1$ states of each isolated vanadium, the above results

show that the spin-orbit coupling generates an easy-plane anisotropy:

$$H_* = \Gamma_{\rm tr}\, S_z^2 \;\simeq\; \frac{\lambda_{\rm SOC}^2}{3V_{\rm tr}}\, S_z^2. \tag{8}$$

We could proceed and consider the effects of a monoclinic distortion $V_m \ll V_{\rm tr}$ that makes the e_g^π orbitals inequivalent and corresponds to an operator [21]

$$\begin{aligned} H_m &= -V_m^{(1)}\,(|a_{1g}\rangle\langle e_{g1}| + |e_{g1}\rangle\langle a_{1g}|) \\ &\quad + V_m^{(2)}\,(|e_{g1}\rangle\langle e_{g2}| + |e_{g2}\rangle\langle e_{g1}|) \\ &= V_m^{(1)}\,(L_xL_z + L_zL_x) \pm V_m^{(2)}\,(L_xL_y + L_yL_x), \end{aligned} \tag{9}$$

where the last expression is the representation on the basis (3). Its action on the $S = 1$ basis $|0\rangle$ and $|\pm1\rangle$ above is equivalent to an additional anisotropy term:

$$\begin{aligned} \delta H_* &= -\frac{\Gamma_m^{(1)}}{2}\,(S_x\,S_z + S_z\,S_x) \\ &\quad \mp \frac{\Gamma_m^{(2)}}{2}\,(S_x\,S_y + S_y\,S_x), \end{aligned} \tag{10}$$

where, if $\xi = (\lambda_{\rm SOC}/3V_{\rm tr})^2 \ll 1$,

$$\begin{aligned} \Gamma_m^{(1)} &= \frac{2V_m^{(1)}}{\sqrt{2}}(\sqrt{2}\,\sin\phi\,\cos\theta - \cos\phi\,\sin\theta) \\ &\simeq 2V_m^{(1)}\,(\xi - 6.5\,\xi^2), \end{aligned} \tag{11}$$

$$\Gamma_m^{(2)} = 2V_m^{(2)}\,\sin^2\phi \simeq 2V_m^{(2)}\,(\xi - 3\,\xi^2), \tag{12}$$

which, together with Eq. (8), might indeed justify the magnetic moment lying in the monoclinic a-c plane, assumed here to be the x-z plane, 29° above the hexagonal basal plane. We cannot extract the value of that angle since the sign-alternating term $\Gamma_m^{(2)}$ competes against the intersite exchange constants, so that we would need the latter to get a reliable estimate.

However, even though the above calculation is a very rough one, still it shows that one can rationalize the observed magnetic anisotropy already at the level of a single vanadium, without invoking the "dimer" as a building block [21]. We finally mention that we cannot exclude further contributions to spin anisotropy coming from Dzyaloshinskii-Moriya (DM) exchange processes [43–47], which could be worth analyzing in the future. We can only state that, because the magnetic phase possesses time reversal times inversion symmetry [20], DM processes will not generate weak ferromagnetism.

V. MODEL STUDIES AND DISCUSSION

In the previous sections, we have shown that the GGA+U accurately accounts for the magnetic, structural, and conducting properties of V_2O_3 in its low-temperature phase. This suggests the possibility of recovering similar results by model calculations within an independent-particle approximation.

A. Preliminary remarks

In their series of papers [12–14], CN&R, besides deriving and analyzing by the mean-field approximation an effective spin-orbital Heisenberg Hamiltonian for coupled spin and orbitally degenerate dimers, see Fig. 3, also performed a Hartree-Fock calculation directly on the Hubbard-type Hamiltonian for the three t_{2g} orbitals [13]. Their results are worth being discussed prior to showing our own. Without including any trigonal crystal-field splitting between e_g^π and a_{1g} orbitals, they could stabilize the "true" magnetic order in two different phases, which they denoted as AO–RS(e_g^π)PS(a_{1g}) and 2RS(e_g^π). The former, AO–RS(e_g^π)PS(a_{1g}), is stable at $J/U \lesssim 0.2$ and is compatible with the "dimer" building block picture of Fig. 3; it has an antiferro-orbital order (AO) in the e_g^π orbital space and the magnetic moment of each vanadium is provided by the unpaired e_g^π electron [RS(e_g^π)], i.e., it is closer to $S = 1/2$, while the a_{1g} is paramagnetic [PS(a_{1g})]. Conversely, the second phase 2RS(e_g^π) at larger J/U is close to the atomic picture of Fig. 1, hence to our previous GGA+U results. It lacks antiferro-orbital order and the occupancy of each a_{1g} orbital is reduced down to $\simeq 0.5$. However, CN&R dismissed such mean-field solution because it has a magnetic moment close to $2\mu_{\rm B}$ [$S = 1$, thence 2RS(e_g^π)], too large with respect to the value $\sim 1.4\mu_{\rm B}$ that was believed correct at that time. In addition, that phase is metallic at the value $U = 2$ eV they considered. A monoclinic distortion might drive a transition into an insulator, but they estimated that a realistic distortion could open a gap ~ 0.05 eV an order of magnitude smaller than the experimental one. Nowadays, we know that the actual spin contribution to the magnetic moment is $\sim 1.7\mu_{\rm B}$, which thus favors rather the 2RS(e_g^π) phase than the AO–RS(e_g^π)PS(a_{1g}) one. In addition, we also know that the trigonal crystal field splitting does contribute substantially to the gap opening [7], hence cannot be neglected as CN&R did.

Since CN&R's seminal papers, all subsequent mean-field calculations have been done on spin-orbital Heisenberg models with nearest-neighbor exchange either within the "dimer" picture [18–21,24] or in the atomic one [20,24]. These approaches implicitly assume Mott's physics, i.e., very large U and J compared to all other Hamiltonian parameters, which we believe it is poorly justified especially for pure V_2O_3 that turns metallic above the Neél temperature. In fact, the outcome of all those calculations is that the "true" magnetic ordering has the lowest energy in a very narrow region of the parameter space, which would make really fortuitous its occurrence in V_2O_3. This is in accordance with the general arguments of Sec. I, according to which the extreme Mott regime would rather favor "simple" or "layered" magnetic orderings. Indeed, our GGA+U analysis suggests that the "true" magnetic structure is stable, and quite robust indeed, as long as $U - J \lesssim 4$ eV. We thus believe that the mapping from the three-band Hubbard model onto an effective Heisenberg model evidently loses important effects that instead are crucial in stabilizing the "true" order.

One of the reasons often invoked to prefer the Heisenberg model in the dimer representation over that in the single-site one is the evidence by Allen [48] that V^{3+} loses its ion identity in all V_2O_3 phases, mainly by nearest-neighbor correlations. Incidentally, we note that Allen's results do not imply that the bond along the dimer direction is better than any of the other three nearest-neighbor bonds within the $a_{\rm H}$-$b_{\rm H}$ plane, unlike what is commonly stated. In reality, a much simpler interpretation of those results might be that V_2O_3 is not enough correlated. Such a conclusion evidently

TABLE II. Symmetry relations of the hopping amplitudes for corundum phase V_2O_3 according to Ref. [13].

	δ_1	δ_2	δ_3	δ_4
$e^\pi_{g1} \to e^\pi_{g1}$	$-\alpha$	$-\frac{1}{4}\alpha + \frac{3}{4}\beta$	$-\frac{1}{4}\alpha + \frac{3}{4}\beta$	μ
$e^\pi_{g2} \to e^\pi_{g2}$	β	$-\frac{3}{4}\alpha + \frac{1}{4}\beta$	$-\frac{3}{4}\alpha + \frac{1}{4}\beta$	μ
$a_{1g} \to a_{1g}$	σ	σ	σ	ρ
$e^\pi_{g1} \to e^\pi_{g2}$	0	$\frac{\sqrt{3}}{4}(\alpha + \beta)$	$-\frac{\sqrt{3}}{4}(\alpha + \beta)$	0
$e^\pi_{g1} \to a_{1g}$	0	$\frac{\sqrt{3}}{2}\tau$	$-\frac{\sqrt{3}}{2}\tau$	0
$e^\pi_{g2} \to a_{1g}$	$-\tau$	$\frac{1}{2}\tau$	$\frac{1}{2}\tau$	0

agrees with our finding that the magnetic and structural properties are faithfully described by GGA+U and suggests that further neighbor correlations might be crucial to stabilize the "true" magnetic structure [24]. We observe that next-nearest-neighbor correlations are partly included already in the "dimer" representation, but evidently they are not enough. In Sec. V C, we shall propose an extension of the effective Heisenberg model with the inclusion of next-nearest-neighbor antiferromagnetic exchange that we believe is better suitable to capture the correct physics at the mean-field level.

B. Hartree-Fock results

An obvious starting point is a three-orbital tight-binding model with only nearest-neighbor hopping for the corundum phase supplied by a local Hubbard U and a Coulomb exchange J. Following Ref. [13], all the required hopping amplitudes for the tight-binding model can be obtained by symmetry considerations from six parameters, as shown in Table II, using the bond nomenclature in Fig. 17. To allow comparison with previous works, we use a set of parameters calculated by Saha-Dasgupta *et al.* [23] in an *N*MTO basis set, which also reproduce well our GGA band structure. They are summarized in Table III. In comparison with other parameters obtained by Refs. [13] and [31], they are characterized by relatively small out-of-plane hopping amplitudes, μ and ρ, as also found in Ref. [49], and by slightly different in-plane values, α and β. According to Ref. [23], the monoclinic distortion would lead to a change up to 4% of the hopping amplitudes, with the possible exception of the out-of-plane ones. We shall therefore not account for those changes and keep using the corundum structure parameters. The two-particle interaction, which includes a Hubbard U and a Coulomb exchange that

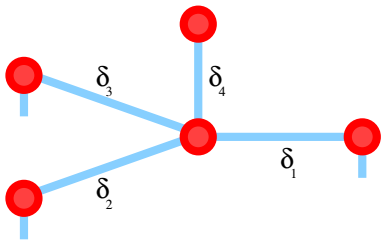

FIG. 17. (Color online) The nearest-neighbor bonds, δ_i, $i = 1, \ldots 4$, see Table II, following the notation of Ref. [13]. δ_4 corresponds to the vanadium dimer, δ_1, δ_2, and δ_3 are the in-plane bonds.

TABLE III. Tight-binding parameters (in eV) obtained for the corundum phase V_2O_3 by Saha-Dasgupta *et al.* [23]. Nomenclature according to Ref. [13].

μ	ρ	$-\alpha$	β	σ	$-\tau$
0.06	−0.51	0.08	−0.21	−0.03	−0.26

we assume equal to $J = U/4$, is treated within the Hartree-Fock approximation. This amounts to considering a trial wave-function ground state of a noninteracting Hamiltonian with the same hopping amplitudes and, in addition, with spin and orbital dependent on-site energies. We shall use an eight-site supercell, which allows us to describe the "true" antiferromagnetic state, so that there are in principle eight sets of Hartree-Fock on-site energies to be determined by minimizing the average total energy.

Figure 18 shows the Hartree-Fock total energies for each of the magnetic configurations that are obtained by a suitable choice of the initial configuration. The comparison with GGA+U in the corundum phase is in fact not bad, despite the roughness of the model Hamiltonian, which we could in principle improve, e.g., accounting for the monoclinic distortion or using more rigorous schemes as in Ref. [50]. In particular, we cannot compare directly the value of U used here with that in GGA+U, which already at $U = 0$ includes correlation effects. Furthermore, since the value of U controls the effective crystal-field splitting and the size of the magnetic exchange equivalently, it is not surprising that the "true" structure remains the lowest energy one. We find that the situation changes, e.g., by assuming a larger bare crystal field, favoring the "simple" two-lattice antiferromagnetism.

Bearing in mind the comparatively large differences between the reported values of the out-of-plane hopping, a first check of the model accuracy is to estimate the influence thereof onto the overall phase stability, which is highlighted in Fig. 19 in the extreme limit of vanishing out-of-plane hopping parameters, $\mu = \rho = 0$. This calculation is also significant since one of the main effects of the monoclinic distortion is tilting and stretching the out-of-plane vanadium dimer bonds, see Fig. 14, thus further reducing the out-of-plane hopping.

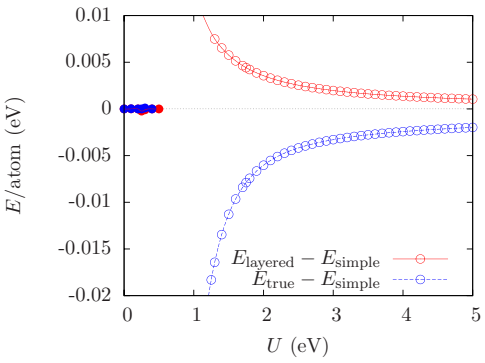

FIG. 18. (Color online) Phase stability from a Hartree-Fock calculation using the tight-binding parameters obtained by Saha-Dasgupta *et al.* [23] for corundum V_2O_3. Closed circles indicate metallic, open circles indicate insulating solutions.

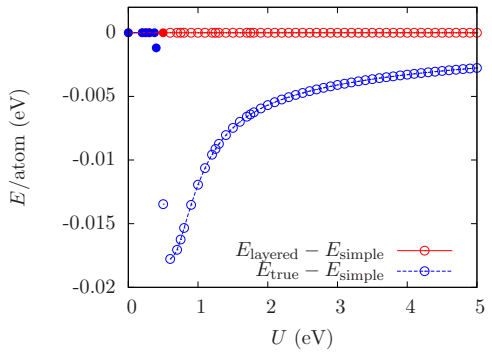

FIG. 19. (Color online) Phase stability from a Hartree-Fock calculation using tight-binding parameters obtained by Saha-Dasgupta *et al.* [23] for corundum V_2O_3, but fixing all hopping perpendicular to the vanadium planes to 0. Closed circles indicate metallic solutions, while open circles indicate insulating solutions.

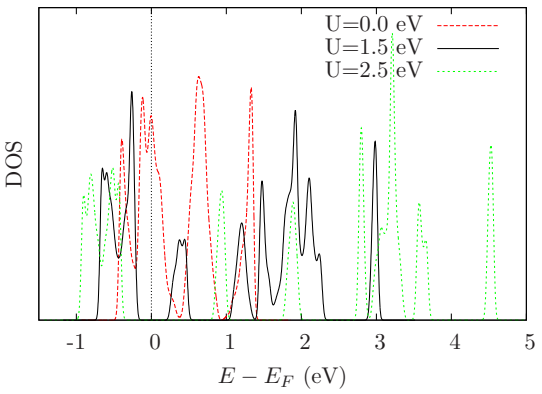

FIG. 21. (Color online) Hartree-Fock density of states of the nonmagnetic metal at $U = 0$ and the "true" antiferromagnetic structure in the insulating regime at $U = 1.5$ and 2.5 eV.

When $\mu = \rho = 0$, the "layered" and "simple" orderings are obviously degenerate, but the "true" one is still stable up to large values of U, although with a smaller energy difference. This suggests that the reason for the stability of the "true" structure is primarily in the in-plane physics. The out-of-plane hopping further stabilizes this phase, at the same time, destabilizing the "layered" structure compared to the "simple" one.

The occupation numbers of the three orbitals on each vanadium site, displayed in Fig. 20, show a very similar behavior to the GGA+U results of Fig. 13, with the exception of the small-U nonmagnetic metal phase. In the intermediate (unphysical) antiferromagnetic metallic regime, one can even see a slight increase of the majority-spin a_{1g} occupations, but a sharp decrease at the metal-insulator transition reveals again the scenario in which the two electrons per site occupy the e_g^π orbitals, making the a_{1g} orbitals practically empty. Note that this orbital polarization turns out to be stronger than in GGA+U, which can be attributed to the fact that the total occupation of the Hartree-Fock model is kept fixed at 2, so that no contributions of, e.g., neighboring oxygen atoms can occur. How to adapt the occupation numbers to compare with experimental findings is shortly discussed in Ref. [7]. We mention that in the insulating regime we also found metastable solutions that correspond to the $S = \frac{1}{2}$ scenario of CN&R orbitals. However, we were unable to find a set of parameters for which such a solution becomes the global energy minimum. Typical energy differences between $S = 1$ and $\frac{1}{2}$ solutions for realistic parameters lie between 0.25 and 0.3 eV per vanadium atom.

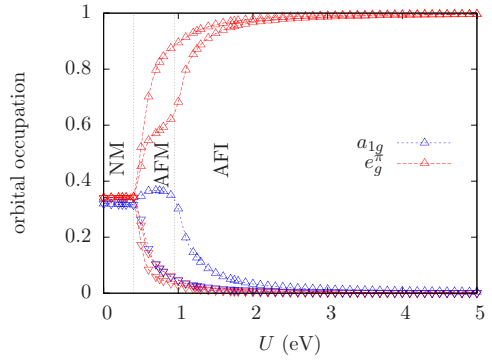

FIG. 20. (Color online) Orbital occupations in the "true" antiferromagnetic phase from Hartree-Fock as a function of U. Triangles pointing up indicate the majority-spin channel, triangles pointing down the minority-spin channel. NM, AFM, and AFI stand for nonmagnetic metal, antiferromagnetic metal, and antiferromagnetic insulator, respectively.

Furthermore, the aforementioned splitting of the e_g^π orbitals shows up also in the "true" antiferromagnetically ordered phase with hopping parameters of the corundum structure, as opposed to the "layered" and "simple" ordering. This is a further evidence that the magnetic order is prone to the structural distortion. We highlight that such a splitting is uniform within all the eight sites of the supercell, as we also found by GGA+U. In other words, both Hartree-Fock approximation and GGA+U predict a ferro-orbital ordering within the e_g^π manifold, unlike the antiferro-orbital one found in Ref. [13], the previously mentioned AO–RS(e_g^π)PS(a_{1g}) phase.

In Fig. 21, we show the density of states of the nonmagnetic metal at $U = 0$ and of the "true" antiferromagnetic structure in the insulating regime at $U = 1.5$ and 2.5 eV. We observe that $U = 1.5$ eV is already enough to open a gap of the right order of magnitude between e_g^π and a_{1g} states, unlike what was found by CN&R without including any trigonal crystal-field splitting. Indeed, the latter is amplified by the Coulomb repulsion and can drive a transition into an insulator by emptying the a_{1g} orbital. This is evident by the Hartree-Fock on-site energy terms, shown in Fig. 22, which display a large increase of the e_g-a_{1g} crystal-field splitting with increasing value of U, especially for the majority spin, whereas all three orbitals are basically unoccupied for the minority spin. Also the splitting of the e_g orbitals is visible, which amounts to the relatively large value of 30 meV for the majority spin in the region of realistic parameter values. We note that the lowering of $e_{g\downarrow}^\pi$ with respect to $e_{g_2}^\pi$ follows from our choice of a specific "true" magnetic order among the three equivalent ones allowed by the original C_3 symmetry.

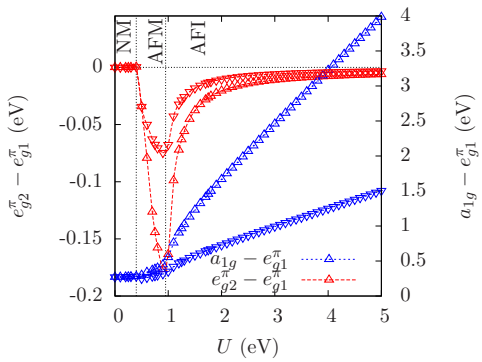

FIG. 22. (Color online) Differences of the on-site energy terms in the "true" antiferromagnetic phase from Hartree-Fock as a function of U. Triangles pointing up indicate the majority spin channel, triangles pointing down the minority spin channel. NM, AFM, and AFI stand for nonmagnetic metal, antiferromagnetic metal, and antiferromagnetic insulator, respectively.

In conclusion, even the Hartree-Fock approximation to a three-band Hubbard model with realistic hopping parameters reproduces the correct magnetic structure and indicates the tendency towards a spontaneous monoclinic distortion. The insulating phase is stabilized at lower values of U than within GGA+U. This is not surprising due to the absence of a possible GGA+U-like double-counting correction, which therein causes a downward shift of the vanadium $3d$ states, leading, typically, but not always [51], to increased hybridization with the lower-lying oxygen $2p$ states.

C. Role of the a_{1g} orbital

Within both GGA+U and Hartee-Fock the effect of U is to increase repulsion between occupied and unoccupied states, hence between majority and minority spins and between e_g^{π} and a_{1g} orbitals. Therefore, at large enough U, the a_{1g} orbital can be discarded and one expects a two-sublattice antiferromagnetic order to prevail. This is indeed the case, see Fig. 11. It thus follows that the a_{1g} orbital, which is indeed depleted but not completely at realistic values of $U - J$, must play a role to stabilize the "true" magnetic ordering. We argue that such a role is to provide magnetic frustration. We already mentioned that the effective Heisenberg models describing nearest-neighbor coupled "dimers" [12,18–21] already account for some of further-neighbor correlations, specifically between two next-nearest-neighbor vanadium atoms lying on adjacent planes. However, our Hartree-Fock result with vanishing out-of-plane hopping amplitudes suggests that further neighbor correlations within the plane are equally important.

Let us imagine that the effective crystal-field splitting, enhanced by U, is large enough that we can treat the hopping τ, see Table III, between e_g^{π} and a_{1g} in perturbation theory. Let us focus on the vanadium atom drawn as a large circle in Fig. 23. At second order, τ induces next-nearest-neighbor e_g^{π}-e_g^{π} hopping terms. They are shown as light blue lines in Fig. 23, and compete against the nearest-neighbor ones, drawn in dark blue. Note that our "true" antiferromagnetic order provides an optimal number of antiferromagnetically coupled "light blue" bonds. If we also take into account the large direct

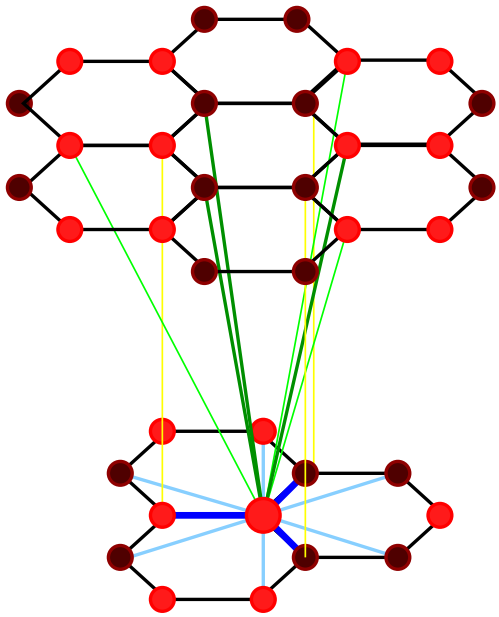

FIG. 23. (Color online) Illustration of the magnetic ordering (different spin directions as light red and dark red) and of the different relevant hopping processes from the central atom shown as a large circle. Besides the nearest-neighbor e_g^{π}-e_g^{π} direct hopping, dark blue, we draw the a_{1g}-mediated next-nearest-neighbor ones: light blue in the hexagonal plane and green between planes. Bold green lines denote that two independent paths produce the same hopping process.

a_{1g}-a_{1g} hopping along the c axis, ρ in Table III, next-nearest-neighbor e_g^{π}-e_g^{π} hopping processes between adjacent planes are generated, see green lines in Fig. 23, where the bold ones indicate that there are two different paths contributing to that process. As we previously said, only the latter processes are taken into account by the Heisenberg model of dimers coupled by nearest-neighbor exchange constants. Note again that the optimal number of antiferromagnetic "bold green" bonds, assuming "true" in-plane order, is given by ferromagnetic dimer bonds.

If we could use these hopping elements to derive an effective $S = 1$ Heisenberg model, we would find on each plane both nearest-, J_1, and next-nearest-, J_2, neighbor exchange constants. In reality, a rigorous approach should include, at the same order in $1/U$, not only the second-neighbor exchange generated by the next-nearest-neighbor hopping process described above, an exchange sometimes called "supersuperexchange" [47], but also high-order frustrating exchange processes [52,53], as well as the reduction of the nearest-neighbor antiferromagnetic J_1 in accordance with the Kanamori-Goodenough-Anderson rules, see, e.g., Ref. [54]. However, our scope here is just to highlight that the "true" magnetic order may naturally arise from a sizable J_2 antiferromagnetic exchange, not to determine precisely the latter as well as J_1. The phase diagram of the $S = 1/2$ J_1-J_2 Heisenberg model on the honeycomb lattice is relatively well known. [55–57] The two-sublattice antiferromagnet is stable for $J_2 \lesssim 0.2J_1$. For $0.2 \lesssim J_2/J_1 \lesssim 0.4$, there seems to be no magnetic order. Finally, for $J_2 \gtrsim 0.4J_1$, the magnetic order is exactly the "true" antiferromagnet, shown in Fig. 23. We cannot exclude

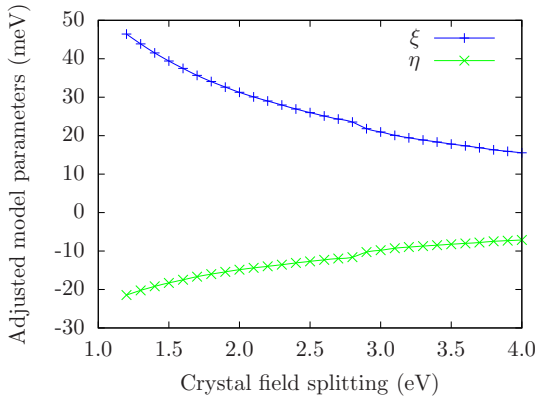

FIG. 24. (Color online) Fitted next-nearest-neighbor in-plane hopping parameters ξ and η of a simplified two-orbital model. See text for details.

that the larger spin $S = 1$ and the coupling between the planes could stabilize in our case the "true" antiferromagnet even in the formerly disordered region $0.2 \lesssim J_2/J_1 \lesssim 0.4$.

In order to give at least a rough estimate on the amount of frustration brought by the a_{1g}-mediated next-nearest-neighbor hopping in terms of the value of J_2, we make use of a more simple model, constructed as follows: we take a two-dimensional honeycomb plane with e_g^π orbitals only as a basis of a tight-binding calculation. The nearest-neighbor hopping of this model shall be equal to the previous calculations, i.e., parametrized by the same parameters $-\alpha = 0.08$ eV and $\beta = -0.21$ eV. Furthermore, we add six next-nearest-neighbor hopping amplitudes per site, which obey the same symmetry relations as the nearest-neighbor ones (the threefold rotational symmetry), and can therefore be parameterized by two parameters in the same way as done for α and β in Table II. We call these two parameters ξ and η, where ξ corresponds to the horizontal $e_{g1}^\pi \rightarrow e_{g1}^\pi$ hopping (similar to $-\alpha$) and η to the $e_{g2}^\pi \rightarrow e_{g2}^\pi$ hopping in the same direction (similar to β). When the crystal field in our original model is large enough, $\gtrsim$1.2 eV, the upper a_{1g}-derived bands are well separated from the lower e_g^π-derived ones near the Fermi energy. We can therefore use the parameters ξ and η directly to fit the band structure of this simple two-band model to the e_g^π-derived bands of the original model. The result is shown in Fig. 24 as a function of an artificial crystal-field splitting of the original model. As expected, ξ and η decrease in absolute value as the crystal field increases. However, for not too large crystal-field splitting, ξ and η have the same order of magnitude as the nearest-neighbor hopping parameters α and β. Now assuming a hypothetical J_1-J_2 Heisenberg model on this fitted two-band dispersion, ξ and η give us an estimate of the next-nearest-neighbor exchange constant J_2 thereof. It can thus at least be assumed to be in the same order of magnitude as the nearest-neighbor exchange J_1. Furthermore, it becomes plausible that it lies in the desired region $J_2 \gtrsim 0.4 J_1$ when extrapolating, knowing that the crystal field is in general not so large that e_g^π and a_{1g} bands are completely separated.

The above calculation is evidently very rough. However, we believe that the overall scenario is correct: the a_{1g} orbital, although pushed by relatively strong correlations above Fermi in the insulating phase, as first noted by DMFT in Ref. [7], still heavily contributes to stabilize the "true" magnetic structure.

VI. CONCLUSIONS

In this work, we have shown that the unusual antiferromagnetic ordering and the monoclinic structural distortion in the low-temperature phase of V_2O_3 are to great extent unrelated phenomena, which simply reinforce each other when they both appear. In particular, we find that the nonmagnetic GGA solution is unstable against a monoclinic distortion, not in disagreement with the recent discovery of a high-pressure nonmagnetic monoclinic phase of V_2O_3 [30]. GGA calculations suggest that such a monoclinic instability is driven by a Fermi surface nesting that increases by electron doping and weakens by hole doping, in accordance with what is observed by chromium versus titanium doping.

As far as the unusual magnetic ordering is concerned, we have identified as main driving mechanism the magnetic frustration brought by the a_{1g} orbitals, which are barely occupied due to the correlation-enhanced crystal-field splitting, yet they contribute to a sizable next-nearest-neighbor antiferromagnetic correlation.

All these features, including the emergence of magnetic anisotropy compatible with the observed orientation of magnetic moments, are well captured by an independent particle scheme as GGA+U in the intermediate-U regime and Hartree-Fock approximation.

ACKNOWLEDGMENTS

We wish to thank S. Shahab Naghavi, Ryan Tyler Requist, Matteo Sandri, Andrea dal Corso, and Erio Tosatti for very helpful discussions. This work has been supported by the European Union, Seventh Framework Programme, under the project GO FAST, Grant Agreement No. 280555.

[1] D. B. McWhan, J. P. Remeika, T. M. Rice, W. F. Brinkman, J. P. Maita, and A. Menth, Phys. Rev. Lett. **27**, 941 (1971).
[2] D. B. McWhan, A. Menth, J. P. Remeika, T. M. Rice, and W. F. Brinkman, Phys. Rev. B **7**, 1920 (1973).
[3] M. Foëx, C. R. Hebd. Seances Acad. Sci. **223**, 1126 (1946).
[4] D. B. McWhan and J. P. Remeika, Phys. Rev. B **2**, 3734 (1970).
[5] R. M. Moon, Phys. Rev. Lett. **25**, 527 (1970).
[6] P. D. Dernier and M. Marezio, Phys. Rev. B **2**, 3771 (1970).
[7] A. I. Poteryaev, J. M. Tomczak, S. Biermann, A. Georges, A. I. Lichtenstein, A. N. Rubtsov, T. Saha-Dasgupta, and O. K. Andersen, Phys. Rev. B **76**, 085127 (2007).
[8] D. Grieger, C. Piefke, O. E. Peil, and F. Lechermann, Phys. Rev. B **86**, 155121 (2012).

[9] S. Y. Ezhov, V. I. Anisimov, D. I. Khomskii, and G. A. Sawatzky, Phys. Rev. Lett. **83**, 4136 (1999).
[10] C. Tenailleau, E. Suard, J. Rodriguez-Carvajal, A. Gibaud, and P. Lacorre, J. Solid State Chem. **174**, 431 (2003).
[11] P. Rozier, A. Ratuszna, and J. Galy, Z. Anorg. Allg. Chem. **628**, 1236 (2002).
[12] C. Castellani, C. R. Natoli, and J. Ranninger, Phys. Rev. B **18**, 4945 (1978).
[13] C. Castellani, C. R. Natoli, and J. Ranninger, Phys. Rev. B **18**, 4967 (1978).
[14] C. Castellani, C. R. Natoli, and J. Ranninger, Phys. Rev. B **18**, 5001 (1978).
[15] K. I. Kugel' and D. I. Khomskii, Sov. Phys. Usp. **25**, 231 (1982).
[16] J.-H. Park, L. H. Tjeng, A. Tanaka, J. W. Allen, C. T. Chen, P. Metcalf, J. M. Honig, F. M. F. de Groot, and G. A. Sawatzky, Phys. Rev. B **61**, 11506 (2000).
[17] L. Paolasini, C. Vettier, F. de Bergevin, F. Yakhou, D. Mannix, A. Stunault, W. Neubeck, M. Altarelli, M. Fabrizio, P. A. Metcalf *et al.*, Phys. Rev. Lett. **82**, 4719 (1999).
[18] F. Mila, R. Shiina, F.-C. Zhang, A. Joshi, M. Ma, V. Anisimov, and T. M. Rice, Phys. Rev. Lett. **85**, 1714 (2000).
[19] S. Di Matteo, N. B. Perkins, and C. R. Natoli, J. Phys.: Condens. Matter **14**, L37 (2002).
[20] S. Di Matteo, N. B. Perkins, and C. R. Natoli, Phys. Rev. B **65**, 054413 (2002).
[21] A. Tanaka, J. Phys. Soc. Jpn **71**, 1091 (2002).
[22] I. S. Elfimov, T. Saha-Dasgupta, and M. A. Korotin, Phys. Rev. B **68**, 113105 (2003).
[23] T. Saha-Dasgupta, O. K. Andersen, J. Nuss, A. I. Poteryaev, A. Georges, and A. I. Lichtenstein, arXiv:0907.2841.
[24] N. B. Perkins, S. Di Matteo, and C. R. Natoli, Phys. Rev. B **80**, 165106 (2009).
[25] S. Di Matteo, Phys. Scr. **71**, CC1 (2005).
[26] K. Held, G. Keller, V. Eyert, D. Vollhardt, and V. I. Anisimov, Phys. Rev. Lett. **86**, 5345 (2001).
[27] J. P. Perdew, K. Burke, and M. Ernzerhof, Phys. Rev. Lett. **77**, 3865 (1996).
[28] P. Giannozzi, S. Baroni, N. Bonini, M. Calandra, R. Car, C. Cavazzoni, D. Ceresoli, G. L. Chiarotti, M. Cococcioni, I. Dabo *et al.*, J. Phys.: Condens. Matter **21**, 395502 (2009), URL http://www.quantum-espresso.org.
[29] P. D. Dernier, J. Phys. Chem. Solids **31**, 2569 (1970).
[30] Y. Ding, C.-C. Chen, Q. Zeng, H.-S. Kim, M. J. Han, M. Balasubramanian, R. Gordon, F. Li, L. Bai, D. Popov *et al.*, Phys. Rev. Lett. **112**, 056401 (2014).
[31] L. F. Mattheiss, J. Phys.: Condens. Matter **6**, 6477 (1994).
[32] V. Eyert, U. Schwingenschlögl, and U. Eckern, Europhys. Lett. **70**, 782 (2005).
[33] D. Grieger and F. Lechermann, Phys. Rev. B **90**, 115115 (2014).
[34] M. Cococcioni and S. de Gironcoli, Phys. Rev. B **71**, 035105 (2005).
[35] P. Pfalzer, G. Obermeier, M. Klemm, S. Horn, and M. L. denBoer, Phys. Rev. B **73**, 144106 (2006).
[36] J. Kündel, P. Pontiller, C. Müller, G. Obermeier, Z. Liu, A. A. Nateprov, A. Hörner, A. Wixforth, S. Horn, and R. Tidecks, Appl. Phys. Lett. **102**, 101904 (2013).
[37] A. Abragam and B. Bleaney, in *Introduction to Ligand Field Theory* (Clarendon Press, Oxford, 1970), pp. 377–378 and 426–429.
[38] G. M. Cole and B. B. Garrett, Inorg. Chem. **9**, 1898 (1970).
[39] O. Tchernyshyov, Phys. Rev. Lett. **93**, 157206 (2004).
[40] N. B. Perkins and O. Sikora, Phys. Rev. B **76**, 214434 (2007).
[41] A. Dal Corso and A. Mosca Conte, Phys. Rev. B **71**, 115106 (2005).
[42] A. I. Liechtenstein, V. I. Anisimov, and J. Zaanen, Phys. Rev. B **52**, R5467 (1995).
[43] I. Dzyaloshinsky, J. Phys. Chem. Solids **4**, 241 (1958).
[44] T. Moriya, Phys. Rev. **120**, 91 (1960).
[45] S. Schuwalow, C. Piefke, and F. Lechermann, Phys. Rev. B **85**, 205132 (2012).
[46] I. V. Solovyev, M. V. Valentyuk, and V. V. Mazurenko, Phys. Rev. B **86**, 054407 (2012).
[47] I. V. Solovyev, Phys. Rev. B **90**, 024417 (2014).
[48] J. W. Allen, Phys. Rev. Lett. **36**, 1249 (1976).
[49] I. V. Solovyev, Phys. Rev. B **73**, 155117 (2006).
[50] I. V. Solovyev, Phys. Rev. B **74**, 054412 (2006).
[51] I. V. Solovyev and K. Terakura, Phys. Rev. B **58**, 15496 (1998).
[52] M. Takahashi, J. Phys. C: Solid State Phys. **10**, 1289 (1977).
[53] A. H. MacDonald, S. M. Girvin, and D. Yoshioka, Phys. Rev. B **37**, 9753 (1988).
[54] J. B. Goodenough, *Magnetism and the Chemical Bond* (Interscience-Wiley, New York, 1963).
[55] J. Fouet, P. Sindzingre, and C. Lhuillier, Eur. Phys. J. B **20**, 241 (2001).
[56] A. F. Albuquerque, D. Schwandt, B. Hetényi, S. Capponi, M. Mambrini, and A. M. Läuchli, Phys. Rev. B **84**, 024406 (2011).
[57] F. Mezzacapo and M. Boninsegni, Phys. Rev. B **85**, 060402 (2012).